

A new parameter identification method of a dual-rotor flux-modulation machine based on an adaptive differential evolution algorithm

Yuan Mao¹ | Shuangxia Niu¹ | Yun Yang² 

¹ Department of Electrical Engineering, The Hong Kong Polytechnic University, Hung Hom, Kowloon 999077, Hong Kong

² Department of Electrical Engineering, The Hong Kong Polytechnic University, Hong Kong and with the Department of Electrical and Electronic Engineering, The University of Hong Kong, Hong Kong

Correspondence

Shuangxia Niu, CF602, Department of Electrical Engineering, The Hong Kong Polytechnic University, Hung Hom, Kowloon, Hong Kong, 999077.
Email: eesxniu@polyu.edu.hk

Funding information

Research Grant Council of the Hong Kong Government, Grant/Award Number: PolyU 152058/17E; Research Grant Council of the Hong Kong Government, Grant/Award Number: PolyU 152058/17E

Abstract

With the wide applications of dual-rotor flux-modulation machines for the growing wind power generations, research activities for the control of dual-rotor flux-modulation machines are intensified in recent years. Most of the existing control schemes are based on indirect measurements of the d-axis inductance, the q-axis inductance and the stator resistance to achieve high torque density and low torque ripple for the dual-rotor flux-modulation machines. However, conventional measurements of the d-axis inductance, the q-axis inductance and the stator resistance may suffer from (i) low accuracy and (ii) additional sensor costs. To this end, an adaptive differential evolution algorithm is proposed to identify the machine parameters by considering the magnetic saturation and cross-coupling issue at low rotational speed of dual-rotor flux-modulation machines. Finite element analysis is adopted in simulation to preliminarily monitor the actual machine parameter values based on the length and cross section area of the conductor and inductance matrix computation. Both simulation and experimental results reveal that the adopted adaptive differential evolution algorithm can identify the three parameters more steadily and accurately than the conventional genetic algorithm.

1 | INTRODUCTION

Owing to the economic viability, matured technology and non-polluting nature, wind energy has become one of the most aspiring renewable energy sources for power grids. For example, European Union's renewable energy directives have already set a goal of producing more than 15% of energy from wind by 2030 [1]. It is expected that more wind energy will be installed for the existing power grids and future smart grids. By far, traditional single-rotor electric machines are most widely used for wind energy conversion systems. However, bulky mechanical gears or even the magnetic gears (MGs) in the single-rotor electric machines may suffer from high acoustic noise, low reliability, weak transmission precision and large total volume and weight [2–5]. To overcome these drawbacks, dual-rotor flux-modulation (DRFM) machines, which integrate both the brushless permanent magnetic (PM) machines and MGs, are proposed [6].

Being different from the traditional single-rotor machines to achieve either energy conversion or speed variation, DRFM machines can implement both functions with even lower costs, more compact structures and smaller volumes [7,8]. They also inherit the merit of the traditional single-rotor machines to operate with higher torque density and better winding heat dissipation performance by adopting PMs as excitation sources, as compared to the traditional wound field machines. Research activities of DRFM machines in various perspectives are intensified over the last decade. Nevertheless, some aspects of DRFM machines have not been fully investigated. One important aspect is the parameter identifications of DRFM machines, which has been rarely studied. It is well known that accurate monitoring the d-axis inductance, q-axis inductance and stator resistance of the DRFM machine can enhance the vector control performance with zero offsets at steady state, fast dynamics and low harmonics [9–12]. These parameters are inherent properties that are correlated to the topology, material,

This is an open access article under the terms of the [Creative Commons Attribution License](https://creativecommons.org/licenses/by/4.0/), which permits use, distribution and reproduction in any medium, provided the original work is properly cited.

© 2021 The Authors. *IET Renewable Power Generation* published by John Wiley & Sons Ltd on behalf of The Institution of Engineering and Technology

winding distribution, and thermal effect of DRFM machines. In general, finite element analysis (FEA) can be used to identify these parameters accurately [13–15]. However, due to the FEA is only validated for electric machines with well-known topologies, it cannot be used to identify the parameters of well-packaged DRFM machines in practice. In this paper, the FEA method is adopted in simulation to identify the d-axis inductance, q-axis inductance and stator resistance of the machine as references for the heuristic algorithm-based method in experiment. Some pioneering identification methods, including the standstill frequency response test [16], the short-circuit test [17], the load rejection test [18] and the current decay test [19], have been adopted for well-packaged wound-field permanent magnet synchronous machines (PMSM). However, these methods are only validated for PMSM without considering the magnet saturation and cross-coupling effects.

To bridge the research gap, owing to the development of digital processors, heuristic algorithm-based methods are used to monitor the parameters of PMSM with the considerations of electromagnetic characteristics in saturation and cross-coupling [20]. In ref. [21] and ref. [22], a particle swarm optimization-based method and a genetic algorithm (GA)-based method are employed to estimate multiple parameters of PMSM based on non-linear state equations. In ref. [23], the GA-based method is further developed to identify both the electromagnetic and mechanical parameters of a PMSM. In ref. [24], flux linkage and dq-axis inductances of a PMSM is accurately monitored by an improved immune clonal-based quantum GA. Besides, the identification performances of various types of GA-based methods are compared in ref. [25].

This paper presents an adaptive differential evolution (ADE)-based method to identify the d-axis inductance, q-axis inductance and stator resistance of a recently proposed bi-directional DRFM machine, which gain the merits of superior torque density and better heat dissipation performances than the traditional wound field machines for wind turbines. ADE is an intuitive, yet powerful evolutionary algorithm to search out global optimal solutions with the smoothest convergence [26,27]. It has been validated to outperform the conventional GA in (i) global optimum rather than local optimum and (ii) fewer tuning parameters by numerous single- and multi-objective problems in different areas [28–34]. In this paper, the ADE algorithm performs more accurate identifications on the three parameters than the conventional GA. The proposed method is established based on the measurements of driving voltages and currents of the DRFM machine at different frequencies. If all the parameters of the machine are well known, the driving voltages (as the system outputs) can be accurately estimated based on the measured driving currents (as the system input) and the mathematical model (as the transfer function of the system). However, some parameters of the well-packaged DRFM machine, such as the d-axis inductance, q-axis inductance and stator resistance, are unknown. Hence, by minimizing the measured driving voltages (as the actual system outputs) and the estimated driving voltages (as the estimated system outputs) based on the measured output currents and the mathematical model, the three unknown parameters can be identified. In other words,

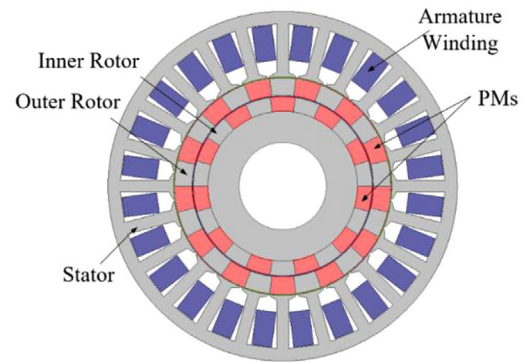


FIGURE 1 Cross section configuration of the dual-rotor flux-modulation machine

the ADE algorithm can search the values of the d-axis inductance, q-axis inductance and stator resistance of the investigated DRFM machine to make sure the differences between the measured driving voltages and the estimated driving voltages are minimized.

The main contributions of this paper include: (1) This might be the first paper to identify the d-axis inductance, q-axis inductance and stator resistance of a recently proposed DRFM machine, which owns the potential of wide applications in wind energy conversion systems. (2) This paper compares the performance of the proposed ADE algorithm and the conventional GA to identify the parameters of a flux-modulation permanent-magnetic machine. (3) Compared to the conventional methods to monitor the parameters of a DRFM machine at high rotational speed [35], the proposed ADE algorithm-based method can identify the parameters at a relatively low rotational speed.

2 | A BRIEF REVIEW OF THE DUAL-ROTOR-FLUX-MODULATION MACHINE

The structure of the investigated DRFM machine is shown in Figure 1, which comprises two rotors and one stator. Both the two rotors are designed as the PM-ferrite array structure. The armature winding is settled in the stator. As shown in Figure 2, both of the inner rotor PM and outer rotor PM have radially outward direction. The magnetic flux can be decomposed into two paths. One path is induced by the inner PM excitation, while the other path is induced by the outer PM excitation. In this machine, the flux modulation effect is achieved in two ways. Both the inner rotor PMs and outer rotor PMs can interact with the windings via the modulation ferrite in another rotor's teeth respectively. Compared with the pure rotor-PM machine and the stator-PM machine, this type of machine is expected to have improved torque density because of its dual PM excitation.

Some major parameters of the DRFM machine are labelled in Figure 3. Detailed information of main design parameters are listed in Table 1. Assume the pole pair number of field excitation exciter is P_f and the modulator pole number is P_r , then the

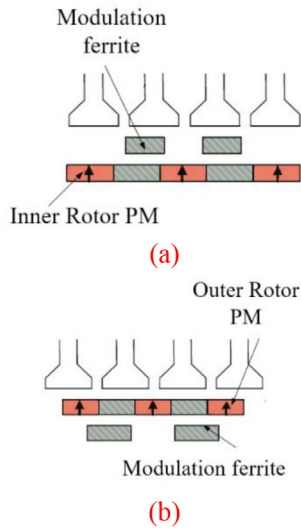


FIGURE 2 Permanent magnetic bi-directional excitation mechanism of the dual-rotor flux-modulation machine. (a) Inner rotor permanent magnetic excitation, (b) outer rotor permanent magnetic excitation

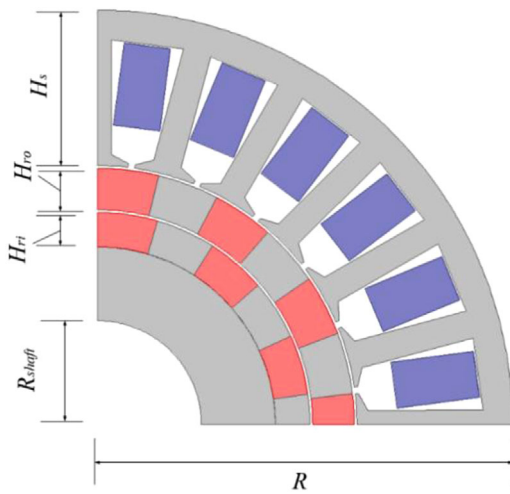


FIGURE 3 Parameters of the dual-rotor flux-modulation machine structure

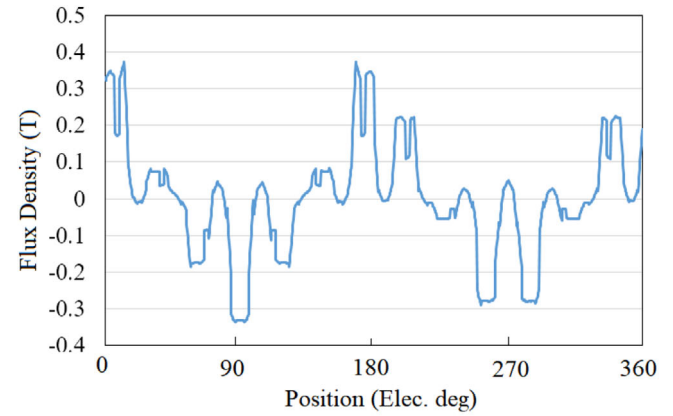
harmonics after modulated $P_{m,k}$ can be drawn as [3]

$$\begin{cases} P_{m,k} = |mP_f + kP_r| \\ m = 1, 3, 5, 7 \dots \quad k = 0, \pm 1, \pm 2 \dots \end{cases} \quad (1)$$

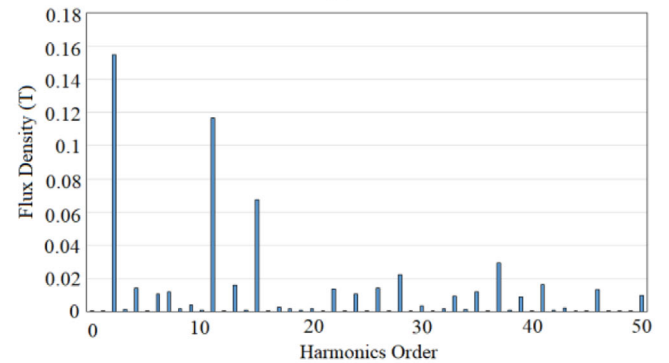
Flux density analysis is conducted by using the FEA. It can be seen from Figure 4 that for the inner PM excitation, the dominant flux harmonics in the airgap is the 2nd-order harmonics. For the outer PM excitation, the dominant flux harmonic is 13th-order harmonics, which is presented in Figure 5. As to realize high transmission ratio, the winding pole pair number is designed to be 2. Therefore, assume ω_{ri} and ω_{ro} represent the angular velocity of inner rotor and outer rotor respectively, then

TABLE 1 Main design parameters

Symbol	Quantity	Value
D	Stator outer diameter	240 mm
R_{shaft}	Shaft radius	30 mm
l_g	Axial length	65 mm
l_{ag}	Airgap length	0.8mm
H_{ri}	Inner rotor height	10 mm
H_{ro}	Outer rotor height	12 mm
H_s	Stator height	45 mm
N_{ri}	Pole pairs of inner rotor	11
N_{ro}	Pole pairs of outer rotor	13
Z	Number of slots	24
P	Number of winding pole pairs	2
N_c	Number of conductors	100
M_r	Magnetic remanence	1.2 T



(a)



(b)

FIGURE 4 Flux density analysis of the inner rotor permanent magnetic excitation. (a) Airgap flux density, (b) spectrum

the speed of armature field ω_a can be derived as

$$\omega_a = \frac{N_{ro}}{N_{ro} - N_{ri}} \omega_{ro} - \frac{N_{ri}}{N_{ro} - N_{ri}} \omega_{ri} \quad (2)$$

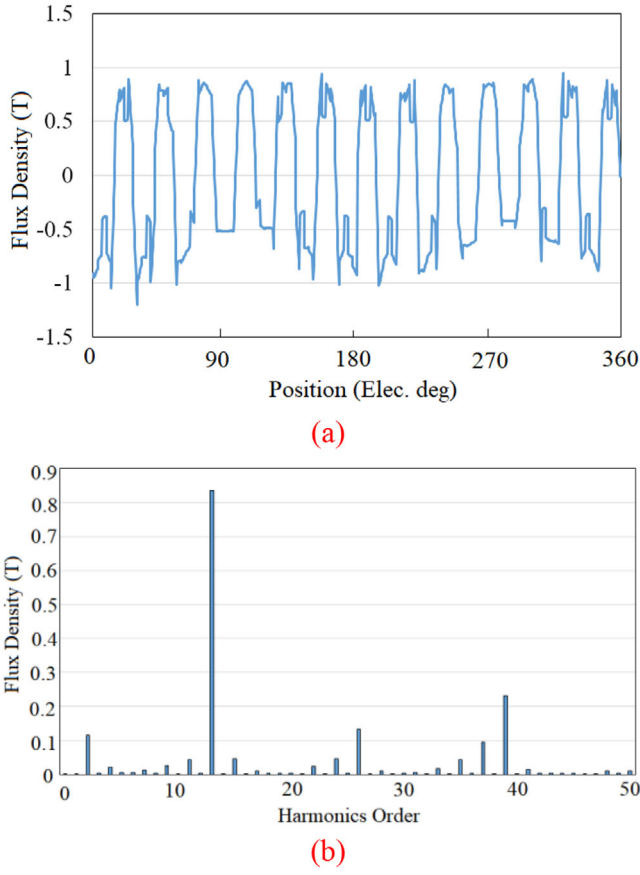


FIGURE 5 Flux density analysis of the outer rotor permanent magnetic excitation. (a) Airgap flux density, (b) spectrum

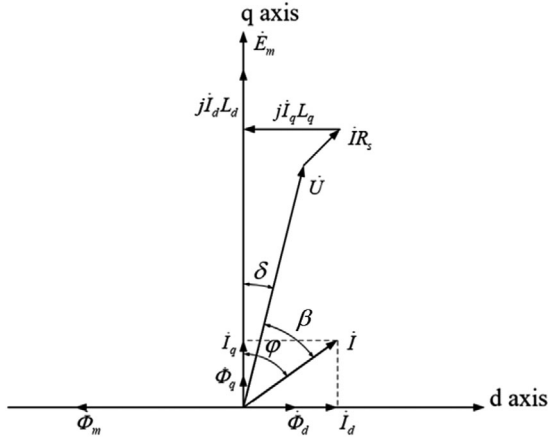


FIGURE 6 Vector diagram of the dual-rotor flux-modulation machine

It can be seen from Equation (2) that this machine can realize a variable transmission ratio. In addition, when the two rotors rotate at different directions to each other, it can achieve relatively high gear ratio.

The vector diagram of the DRFM machine with load is shown in Figure 6. The length of the vector indicates the magnitude the electrical property. The angle difference between the

two vectors indicates the initial phase difference between the two electrical properties. The initial position of the back EMF vector \dot{E}_m is on the q-axis. The initial angle difference between the current vector \dot{I} and \dot{E}_m is the internal power factor angle φ . Then, the d-axis current \dot{I}_d and the q-axis current \dot{I}_q are

$$\begin{cases} \dot{I}_d = \dot{I} \sin \varphi \\ \dot{I}_q = \dot{I} \cos \varphi \end{cases} \quad (3)$$

The equivalent circuit model can be derived as

$$\dot{E}_m = \dot{U} + \dot{I}R_s + j\dot{I}_dL_d + j\dot{I}_qL_q. \quad (4)$$

The angle difference between the voltage vector \dot{U} and the current vector \dot{I} is the external power factor angle β , which can be externally measured. The angle difference between the voltage vector \dot{U} and the back EMF vector \dot{E}_m is the power angle δ , which satisfy

$$\delta = \varphi - \beta. \quad (5)$$

By ignoring the eddy current and hysteresis losses, the flux linkage model of DRFM machine can be formatted as,

$$\begin{cases} \dot{\Phi}_d = L_d \dot{I}_d + \dot{\Phi}_m \\ \dot{\Phi}_q = L_q \dot{I}_q \end{cases} \quad (6)$$

where $\dot{\Phi}_d$ and $\dot{\Phi}_q$ are the d-axis and q-axis flux linkage vectors; $\dot{\Phi}_m$ is the PM flux linkage vector. Substitute Equation (6) into Equation (4), the voltage mathematical model of the DRFM machine can be derived as

$$\begin{cases} \dot{U}_d = R_s \dot{I}_d + p\dot{\Phi}_d - (N_{ro}\omega_{ro} - N_{ri}\omega_{ri})\dot{\Phi}_q \\ \dot{U}_q = R_s \dot{I}_q + p\dot{\Phi}_q + (N_{ro}\omega_{ro} - N_{ri}\omega_{ri})\dot{\Phi}_d \end{cases} \quad (7)$$

where \dot{U}_d and \dot{U}_q are the d-axis and q-axis voltage vectors; p is the differential operator.

3 | THE ALGORITHM OF ADAPTIVE DIFFERENTIAL EVOLUTION FOR THE DUAL-ROTOR-FLUX-MODULATION MACHINE

Based on the time-domain voltage mathematical model in Equation (7), the frequency-domain voltage mathematical model of the DRFM machine can be derived as

$$\begin{cases} u_d = R_s i_d + j\omega(L_d i_d + \varphi_m) - N_s \omega L_q i_q \\ u_q = R_s i_q + j\omega L_q i_q + N_s \omega(L_d i_d + \varphi_m) \end{cases} \quad (8)$$

Obviously, u_d and u_q can be estimated based on the parameters R_s , L_d , L_q , N_s , φ_m , ω , and the measured i_d and i_q , such that

$$\begin{cases} \mathbf{u}_{\text{dest}} = R_s \mathbf{i}_d + j\omega(L_d \mathbf{i}_d + \mathbf{m}) - N_s \omega L_q \mathbf{i}_q \\ \mathbf{u}_{\text{qest}} = R_s \mathbf{i}_q + j\omega L_q \mathbf{i}_q + N_s \omega(L_d \mathbf{i}_d + \mathbf{m}) \end{cases} \quad (9)$$

where $\mathbf{u}_{\text{dest}} = [u_{\text{dest}1} \ u_{\text{dest}2} \ \dots \ u_{\text{dest}n}]^T$; $\mathbf{u}_{\text{qest}} = [u_{\text{qest}1} \ u_{\text{qest}2} \ \dots \ u_{\text{qest}n}]^T$; $\mathbf{i}_d = [i_{d1} \ i_{d2} \ \dots \ i_{dn}]^T$, $\mathbf{i}_q = [i_{q1} \ i_{q2} \ \dots \ i_{qn}]^T$; $\boldsymbol{\varphi}_m = [\varphi_{m1} \ \varphi_{m2} \ \dots \ \varphi_{mn}]^T$. The angular frequency ω is swept from the lower bound ω_L to the upper bound ω_H for the system to obtain various values of u_d , u_q , i_d and i_q . Then, the identification model for the parameters of the DRFM machine can be derived as

$$\begin{aligned} \min J &= \|\mathbf{u}_{\text{dest}} - \mathbf{u}_d\| + \|\mathbf{u}_{\text{qest}} - \mathbf{u}_q\| \\ \text{s.t.} \quad &\begin{cases} \omega_L \leq \omega \leq \omega_H \\ L_{dL} \leq L_d \leq L_{dH} \\ L_{qL} \leq L_q \leq L_{qH} \\ R_{sL} \leq R_s \leq R_{sH} \end{cases} \end{aligned} \quad (10)$$

where $\mathbf{u}_d = [u_{d1} \ u_{d2} \ \dots \ u_{dn}]^T$; $\mathbf{u}_q = [u_{q1} \ u_{q2} \ \dots \ u_{qn}]^T$; L_{dL} , L_{qL} and R_{sL} are the lower bounds of L_d , L_q and R_s , respectively; L_{dH} , L_{qH} and R_{sH} are the upper bounds of L_d , L_q and R_s , respectively. The objective of the identification model in Equation (8) is to minimize the norm of the voltage differences between the estimated \mathbf{u}_{dest} and \mathbf{u}_{qest} , and the measured \mathbf{u}_d and \mathbf{u}_q . The identified parameters L_d , L_q and R_s are searched within the bounds. Based on the identification model, both the conventional GA and the proposed ADE are adopted in this paper to minimize the objective function in Equation (10), thus monitoring L_d , L_q and R_s of the DRFM machine.

The flowchart of the conventional GA is shown in Figure 7. Initially, the individuals, being encoded in strings of bits (0 s and 1 s), also known as the chromosomes, are randomly generated for each parameter (L_d , L_q and R_s) with the population size of P_{size} . Each chromosome contains C_{size} bits. Then, by decoding the binary chromosomes into the decimal solutions, the objective function

$$J = \|\mathbf{u}_{\text{dest}} - \mathbf{u}_d\| + \|\mathbf{u}_{\text{qest}} - \mathbf{u}_q\| \quad (11)$$

can be evaluated based on the decimal individuals. If either of the terminal conditions of (i) the generations reaching the maximum generations max_{gen} or (ii) the algorithm being convergent, is satisfied, the algorithm stops and output the optimum solutions and the corresponding fitness value. On the contrary, if none of the terminal conditions is satisfied, the algorithm goes to the operations of selection, crossover and mutation. For the selection operation, first two parent chromosomes in the current population are selected based on the sorted fitness (greater opportunities to be selected in the roulette for smaller fitness). For the crossover operation, two selected parent chromosomes

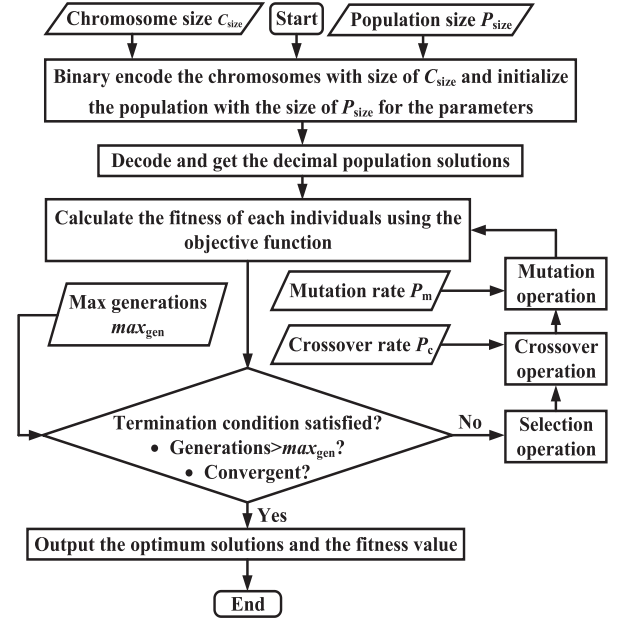


FIGURE 7 Flowchart of the conventional genetic algorithm

cross over at every two loci (positions in two chromosomes) to generate an offspring with the crossover rate of P_c . If no crossover operation is performed, the parent chromosomes are copied. For the mutation operation, the new offspring mutates at each locus (position in the chromosome) to generate another offspring with the mutation rate of P_m . If no mutation operation is performed, the parent chromosome is copied. Then, the newly generated population is applied for the next iteration.

ADE, as a stochastic direct search and global optimization algorithm developed by Storn and Price for continuous space optimization, can overcome the drawbacks of the conventional GA [27]. The advantages of ADE over the conventional GA can be concluded as follows [28–33]:

- 1) ADE can avoid being trapped in local optimum and outperforms conventional GA regarding single-objective and multiple-objective optimization problems;
- 2) ADE uses fewer tuning parameters than conventional GA. Only population size, maximum generation, differential weight (F) bounds and crossover rate (CR) bounds are adopted without resorting to an external probability density function;
- 3) ADE exhibits better performance in exploration and exploitation by dynamically adjusting F and CR.

The flowchart of the ADE algorithm is shown in Figure 8. The process can be described in detail as following:

1. [Initialization]: Generate a random population of P_{size} individuals in the search-space (within the lower and the upper bounds given in Equation (10)) for the parameters of L_d , L_q and R_s .
2. [Fitness]: Evaluate the fitness of each individual using the objective function $J = \|\mathbf{u}_{\text{dest}} - \mathbf{u}_d\| + \|\mathbf{u}_{\text{qest}} - \mathbf{u}_q\|$.

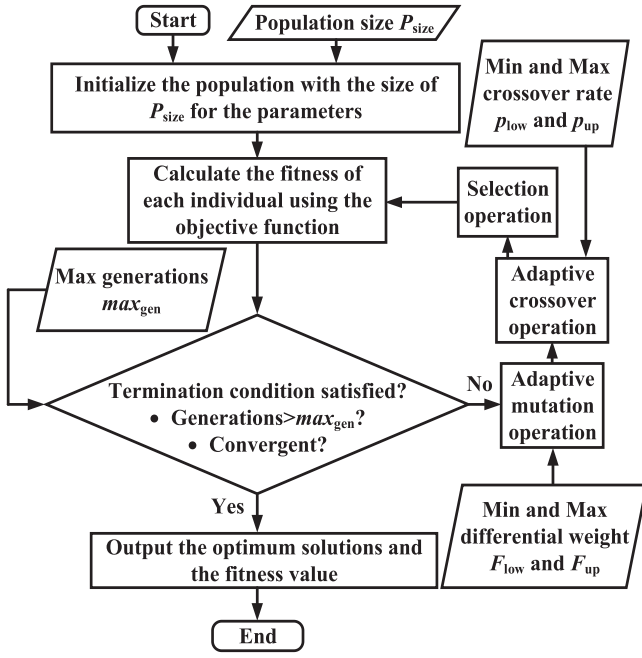


FIGURE 8 Flowchart of the proposed adaptive differential evolution

3. [Checked]: If both the termination conditions of (i) generations reaching the maximum generations \max_{gen} and (ii) the algorithm being convergent, are satisfied, the algorithm stops and output the optimum solutions and the corresponding fitness value. On the contrary, if any one of the termination conditions is not satisfied, the algorithm repeats in the adaptive mutation operation, the adaptive crossover operation and the selection operation.
4. [New population]: Create a new population by repeating the following steps
 1. [Adaptive mutation operation]: Randomly select three vectors of $X_{p1}(g)$, $X_{p2}(g)$ and $X_{p3}(g)$ with distinct indices of p_1 , p_2 , p_3 , where g indicates the number of the iterations. Then, apply the three vectors into the adaptive function

$$F_{\alpha} = F_{low} + (F_{up} - F_{low}) \frac{f_2 - f_1}{f_3 - f_1}. \quad (12)$$

where F_{α} is the adaptive differential weight; F_{low} and F_{up} are the lower and upper bounds of the differential weight, respectively; f_1 , f_2 and f_3 are the fitness of $X_{p1}(g)$, $X_{p2}(g)$ and $X_{p3}(g)$, $f_1 < f_2 < f_3$. Consequently, a new offspring using the differential strategies of DE/rand/1 can be obtained as

$$H_{\alpha}(g) = X_{p1}(g) + F_{\alpha}(X_{p2}(g) - X_{p3}(g)). \quad (13)$$

where $H_{\alpha}(g)$ is the yield of offspring. If $H_{\alpha}(g)$ is invalid, the adaptive mutation operation needs to be performed again until it is in the search-space.

1. [Adaptive crossover operation]: Cross over the two selected parents to generate a new offspring $H_{\alpha}(g)$

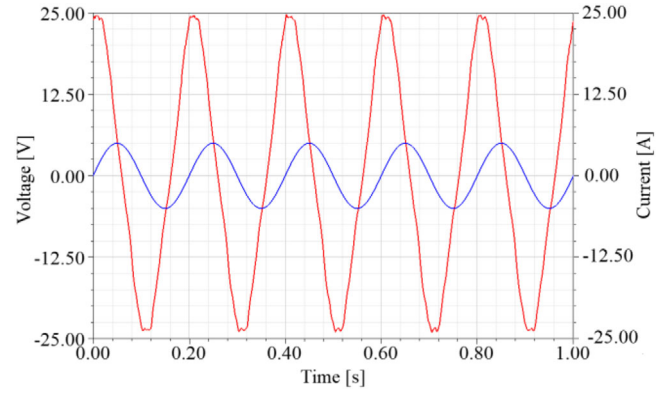


FIGURE 9 Waveforms of the line voltage and current (phase A) at 5 Hz

with the crossover rate $P_{c\alpha}$,

$$P_{c\alpha} = \begin{cases} R_{low} + \frac{(R_{up} - R_{low})(f_{\alpha} - f_{min})}{(f_{max} - f_{min})} & f_{\alpha} < f \\ R_{low} & f_{\alpha} \geq f \end{cases}. \quad (14)$$

where P_{low} and P_{up} are the lower and upper bounds of the crossover rate; f_{α} is the fitness of the individual α ; f_{min} and f_{max} are the minimum and the maximum fitness; f is the averaged fitness. If $r_{\alpha} < P_{c\alpha}$ or $\alpha = R$, where r_{α} is a random number; R is a random index for dimensionality, then set

$$H_{\alpha}(g) = X_{p1}(g) + F_{\alpha}(X_{p2}(g) - X_{p3}(g)). \quad (15)$$

If no crossover operation is performed, the parents are copied.

3. [Selection operation]: Compare $J(X_{\alpha+1})$ to $J(X_{\alpha})$. If $J(X_{\alpha+1}) < J(X_{\alpha})$, then replace the solution in the current population by the improved candidate solution $X_{\alpha+1}$ based on the greedy selection method.
4. [Replace and loop]: If the termination conditions are not satisfied, the algorithm goes to the operations of the adaptive mutation, the adaptive crossover, and the selection, to generate a new population for a further run.

4 | SIMULATION RESULTS

Simulation are carried out using the software Ansys Maxwell and Matlab. The main design parameters of the investigated DRFM machine are listed in Table 1. The frequency of the armature winding field f_s is swept from 5 to 55 Hz with the interval of 5 Hz. The plots of the line voltages and currents (phase a) at 5 Hz are presented in Figure 9. Second-order band-pass filters are used to obtain the fundamental components of both the line voltages and currents. The transfer function of the bandpass filters is

$$H(s) = \frac{2\zeta\omega_0 s}{s^2 + 2\zeta\omega_0 s + \omega_0^2}. \quad (16)$$

TABLE 2 Measurements at different frequencies

f_s (Hz)	δ (deg)	β (deg)	I_d (A)	I_q (A)	U_d (V)	U_q (V)	φ_m (Wb)
5	-54.73	71.27	4.05	-2.94	18.86	13.34	0.88
10	-54.73	71.27	4.05	-2.94	37.72	26.68	0.88
15	-55.17	70.83	4.05	-2.94	56.87	39.57	0.88
20	-55.63	70.37	4.05	-2.94	76.23	52.14	0.88
25	-56.08	69.92	4.05	-2.94	95.78	64.41	0.88
30	-56.53	69.47	4.05	-2.94	115.51	76.37	0.88
35	-57	69	4.05	-2.94	135.43	87.95	0.88
40	-57.43	68.57	4.05	-2.94	155.45	99.30	0.88
45	-57.88	68.12	4.05	-2.94	175.65	110.27	0.88
50	-58.33	67.67	4.05	-2.94	196.02	120.92	0.88
55	-58.80	67.20	4.05	-2.94	216.41	131.06	0.88

TABLE 3 Parameters of the conventional GA

Parameter	Value
Population size P_{size}	12
Maximum generation max_{gen}	1000
Mutation rate	0.2
Crossover rate	0.9
Selection rate	0.5

where the damping ratio ζ is calculated based on the centre frequency (i.e. f_s) and the bandwidth of the bandpass filter (i.e. BW). In this paper, the bandwidth is set to be 10% of the centre frequency, which exhibits good enough filtering performance in both simulation and experiment. Based on the definition as

$$\zeta = \frac{BW}{2f_s}. \quad (17)$$

the damping ratio used in this paper is 0.05.

Based on the amplitudes of the fundamental voltages and currents, and their phase differences, U_d , U_q , I_d and I_q (amplitude values) of the DRFM machine for different f_s can be obtained, as listed in Table 2. The flux produced by PM (φ_m) is preliminarily estimated by the analytical method, which is about 0.88 Wb. The three parameters are initially identified by the 2D FEA solver in Ansys Maxwell. The stator resistance of the machine can be calculated based on the length and cross section area of the conductor. The d-axis inductance and q-axis inductance can be obtained by employing the inductance matrix computation. The d-axis inductance, q-axis inductance and stator resistance are calculated to be $61.42 \mu\text{H}$, $61.46 \mu\text{H}$ and 2Ω , respectively.

The three parameters are identified by the conventional GA and the proposed ADE, the specifications of which by taking both optimization accuracy and computation time into consideration, are provided in Tables 3 and 4, respectively. The searching constraints of the monitored parameters are identically designed for the conventional GA and the ADE, are listed in Table 5.

TABLE 4 Parameters of the ADE

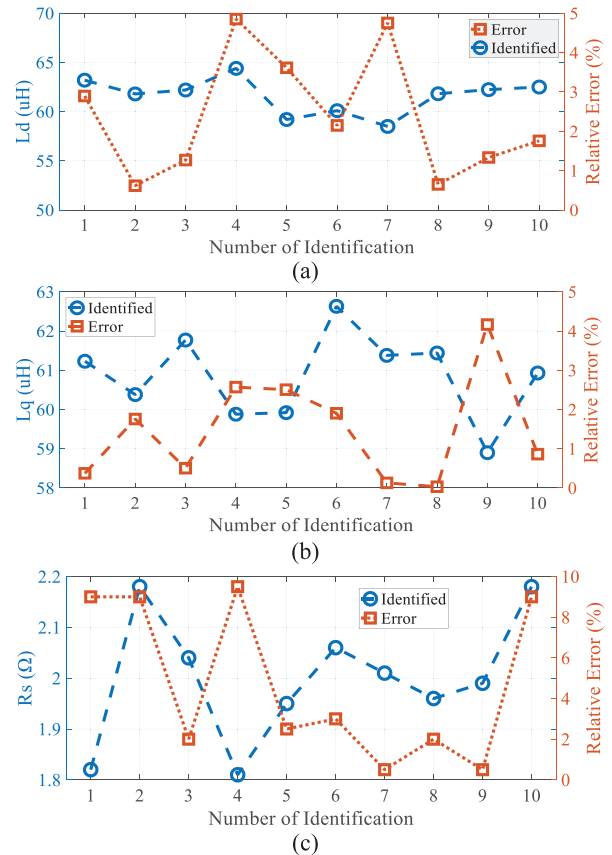
Parameter	Value
Population size P_{size}	18
Maximum generation max_{gen}	400
Lower limit of the differential weight F_{min}	0.1
Upper limit of the differential weight F_{max}	0.8
Lower limit of the crossover rate P_{min}	0.1

TABLE 5 Constraints of the parameters

Lower bounds	Value	Upper bounds	Value
L_{dL}	$40 \mu\text{H}$	L_{dH}	$80 \mu\text{H}$
L_{qL}	$40 \mu\text{H}$	L_{qH}	$80 \mu\text{H}$
R_{sL}	0Ω	R_{sH}	5Ω

4.1 | Conventional genetic algorithm

The parameters are monitored by the conventional GA ten times independently. The comparisons between the identified and the actual parameters of L_d , L_q and R_s , and their relative errors are shown in Figure 10(a)–(c), respectively. The

**FIGURE 10** Identified results of the conventional GA. (a) d-axis inductance, (b) q-axis inductance, (c) stator resistance

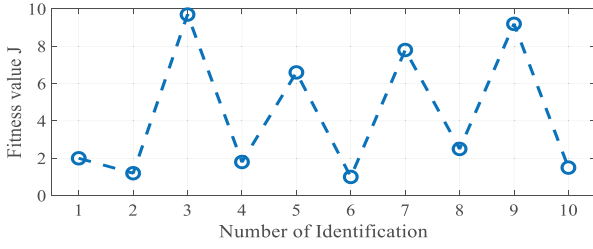


FIGURE 11 Fitness values of the conventional genetic algorithm

maximum relative error of L_d , L_q and R_s can reach about 4.85%, 4.17% and 9.5%, respectively. Despite the relative errors of the identified L_d and L_q are within 5% and the identified R_s are within 10% by the conventional GA, the variations for the 10 cases of identifications are significant. The percentages of the standard deviations over the actual values of the parameters monitored by FEA are 2.96%, 1.77% and 6.3%, respectively. The corresponding fitness values are depicted in Figure 11. Obviously, the fitness values are unsteady, which exhibits the drawbacks of the conventional GA to find local optimal points.

4.2 | Adaptive differential evolution

Then, the three parameters are identified by the ADE with the population size of $P_{size} = 7 * nvar$ ($nvar$ indicates the number of variables to be identified, e.g. $nvar = 3$) ten times independently. The generations of the ADE are converged at 233 for all the 10 cases. The parameters are steadily identified at the generations of 233, 500 and 2000, as shown in Figure 12 (only case 1 is exhibited, the rest cases are similar). The maximum relative error of the parameters identified by the ADE are 0.4%, 0.08% and 0.76%, all of which are less than 1%. The percentages of the standard deviations over the actual values of the parameters monitored by FEA are less than 0.5%. The fitness values of the ADE for all the cases are consistently 0.92, which indicates the ADE can find the global optimal points.

The comparisons of maximum relative error, average relative error and standard deviations of the three identified parameters for all the 10 cases between the conventional GA and the ADE are depicted in Figure 13. The maximum relative error can be reduced about 4.45%, 4.09% and 8.74% for the d-axis inductance, q-axis inductance and stator resistance, as shown in Figure 13(a). The average relative error can be reduced about 1.67%, 1.12% and 4.15% for the three parameters, as shown in Figure 13(b). The standard deviations can be reduced about 2.73%, 1.59% and 5.86% for the three parameters, as shown in Figure 13(c). Apparently, the ADE can identify the three parameters more accurately and steadily than the conventional GA.

5 | EXPERIMENTAL VERIFICATIONS

Experiments are carried out on the prototype of the DRFM machine in Figure 14. The main design specifications of the machine are listed in Table 1. The DRFM machine operates

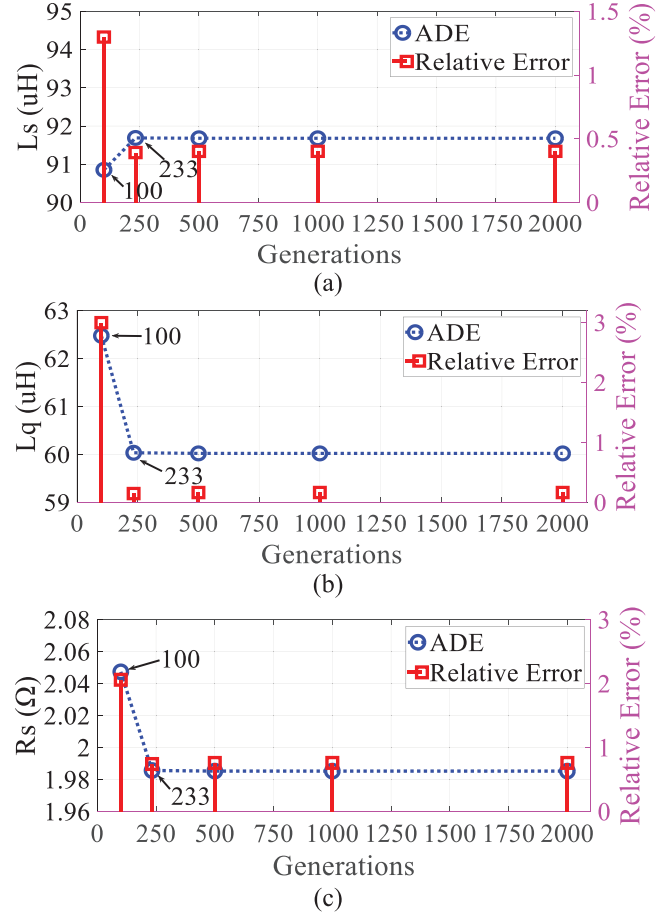


FIGURE 12 Identified results of the adaptive differential evolution. (a) d-axis inductance, (b) q-axis inductance, (c) stator resistance

under both no-load condition and full-load condition to obtain all necessary data. Two sets of servo systems are connected to the two rotors, as shown in Figure 15. TMS320F28335 is adopted as the controller for driving circuit of the DRFM machine. The total costs of the adopted system are about 40,000 Hong Kong dollars, including the costs on the prototype, driving circuits and sensors.

The parameters L_d , L_q and R_s are identified by both the conventional GA and the ADE algorithms in Figures 7 and 8 ten times independently based on the measurements of U_d , U_q , I_d and I_q . The actual L_d , L_q and R_s are assumed to be the same as the parameters given in the simulation, that is, $L_d = 61.42 \mu\text{H}$, $L_q = 61.46 \mu\text{H}$ and $R_s = 2 \Omega$. Then, the comparisons of the identified parameters between the conventional GA and the ADE can be obtained, as shown in Figure 16.

The average relative errors of the three parameters are 12.8%, 12.6% and 10.4% for the conventional GA, while they are only 5.2%, 5.1% and 4.2% for the ADE. The average relative error of the three parameters can be reduced about 7.6%, 7.5% and 6.2%, respectively. The percentages of the standard deviations over the actual values of the parameters are 4.2%, 3.2% and 10.9% for the conventional GA, while they are only 0.8%, 0.3% and 1% for the ADE. The standard deviations can be reduced about 3.4%, 2.9% and 9.9%, respectively. The fitness values of

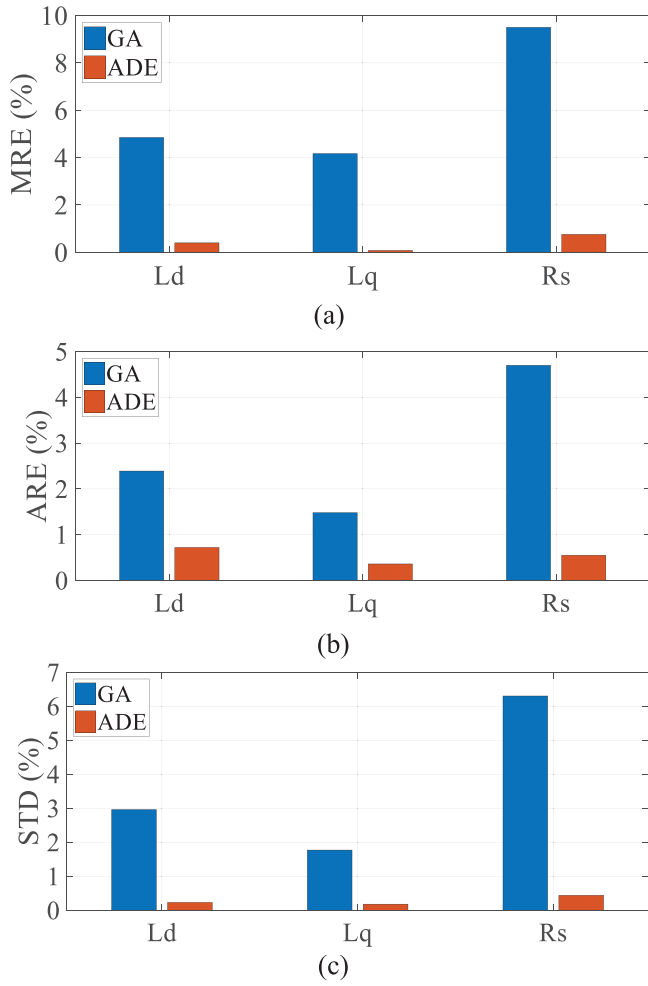


FIGURE 13 Comparisons between genetic algorithm and adaptive differential evolution in simulation. (a) Maximum relative error, (b) average relative error, (c) standard deviations

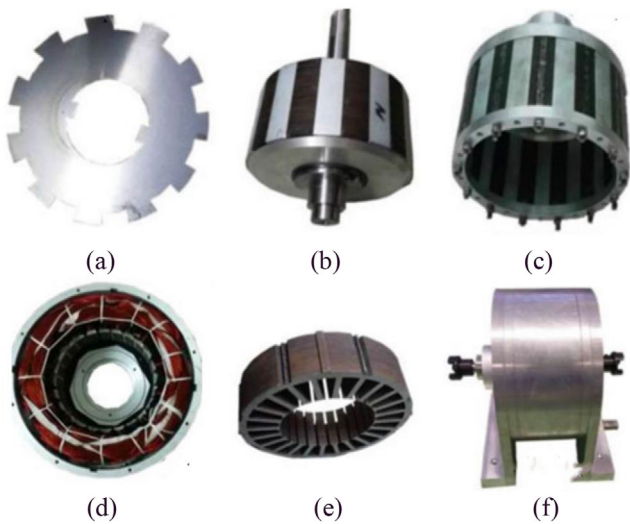


FIGURE 14 Photograph of the machine prototype. (a) Lamination core, (b) inner rotor, (c) outer rotor, (d) armature winding, (e) stator slot, (f) overall appearance

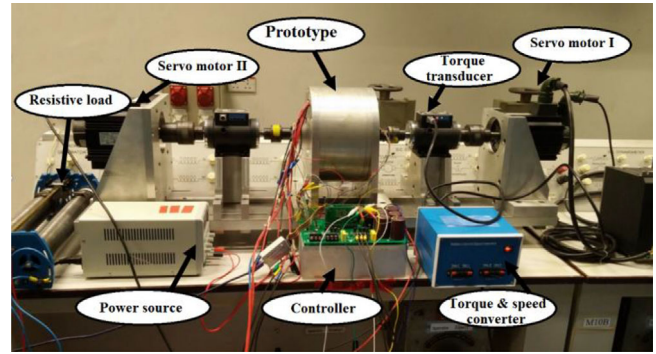


FIGURE 15 Photograph of the test bench

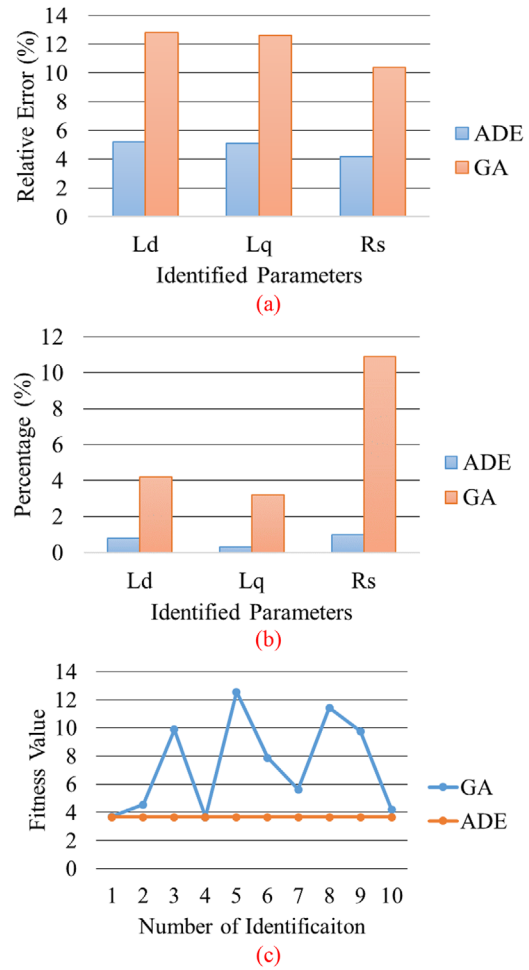


FIGURE 16 Comparisons between genetic algorithm and adaptive differential evolution in experiment. (a) Average relative error, (b) standard deviations, (c) fitness values

the conventional GA are different for all the ten times identifications, while that of the ADE are consistent to be 3.67. The comparisons in Figure 16 validate that the ADE can identify the three parameters more accurately and steadily than the conventional GA for a practical DRFM machine.

6 | CONCLUSIONS

This paper presents an ADE algorithm to identify the parameters of the d-axis inductance, q-axis inductance and the stator resistance of a recently proposed bi-directional DRFM machine. Both simulation and experimental results reveal that the ADE algorithm can identify the three parameters more accurately and steadily than the conventional GA. For the practical DRFM machine, the average relative error of the d-axis inductance, q-axis inductance and the stator resistance can be reduced about 7.6%, 7.5% and 6.2% and the percentages of the standard deviations over the actual values of the parameters can be mitigated about 3.4%, 2.9% and 9.9% by adopting the ADE rather than the conventional GA.

ACKNOWLEDGMENTS

This work is supported by the Research Grant Council of the Hong Kong Government under project PolyU 152058/17E.

ORCID

Yun Yang  <https://orcid.org/0000-0002-0097-9058>

REFERENCES

- 2030 energy strategy: <http://ec.europa.eu/energy/node/163>. Accessed 4 Feb 2016
- Ribrant, J., Bertling, L.M.: Survey of failures in wind power systems with focus on Swedish wind power plants during 1997–2005. *IEEE Trans. Energy Convers.* 22(1), 167–173 (2007)
- Niu, S., Ho, S.L., Fu, W.N.: A novel double-stator double-rotor brushless electrical continuously variable transmission system. *IEEE Tran. Mag.* 49(7), 3909–3912 (2013)
- Liu, C.T., Chung, H.Y., Hwang, C.C.: Design assessments of a magnetic-gear double-rotor permanent magnetic generator. *IEEE Tran. Mag.* 50(1), 4001004 (2014)
- Druant, J., et al.: Torque analysis on a double rotor electrical variable transmission with hybrid excitation. *IEEE Tran. Ind. Electron.* 64(1), 60–68 (2017)
- Bai, J., et al.: Characteristic analysis and verification of the magnetic-field-modulated brushless double-rotor machine. *IEEE Tran. Ind. Electron.* 49(3), 1231–1241 (2013)
- Zhang, Z., et al.: Nonlinear direct control for three-level NPC back-to-back converter PMSG wind turbine systems: Experimental assessment with FPGA. *IEEE Tran. Ind. Informat.* 13(3), 1172–1183 (2017)
- Wang, Y., Niu, S., Fu, W.N.: An electrical-continuously variable transmission system based on doubly-fed flux-bidirectional modulation. *IEEE Tran. Ind. Electron.* 64(4), 2722–2731 (2017)
- Sun, L., et al.: Motion control and performance evaluation of a magnetic-gear dual-rotor in hybrid powertrain. *IEEE Tran. Ind. Electron.* 64(3), 1863–1872 (2017)
- Ahn, H.J., Lee, D.M.: A new bumpless rotor-flux position estimation scheme for vector-controlled washing machine. *IEEE Tran. Ind. Informat.* 12(2), 466–473 (2016)
- Sant, A.V., et al.: Four-axis vector controlled dual-rotor PMSM for plug-in electric vehicles. *IEEE Tran. Ind. Electron.* 62(5), 3202–3212 (2015)
- Sun, L., et al.: Analysis and control of complementary magnetic-gear dual-rotor motor. *IEEE Tran. Ind. Electron.* 63(11), 6715–6725 (2016)
- Lehikoinen, A., Arkkio, A.: Efficient finite-element computation of circulating currents in thin parallel strands. *IEEE Tran. Mag.* 52(3), 1–4 (2016)
- Gyselinck, J., Sabariego, R., Dular, P.: Time-domain homogenisation of windings in 2-D finite element models. *IEEE Tran. Mag.* 43(4), 1297–1300 (2007)
- Rosset, G., Xuan, T., Simond, J.J.: Finite element model of electrical machines coupled to the grid simulation software. *IEEE Tran. Energy Convers.* 26(4), 1127–1133 (2011)
- Yuan, L., et al.: Determination of high-frequency d- and q-axis inductances for surface-mounted permanent-magnet synchronous machines. *IEEE Tran. Instrum. Meas.* 59(9), 2376–2382 (2010)
- Ghomi, M., et al.: Review of synchronous generator parameters estimation and model identification. *Universities Power Engineering Conf.* pp. 228–235 (2007)
- Mello, D., Ribeiro, F.P.: Derivation of synchronous machine parameters from tests. *IEEE Tran. Power Apparatus Syst.* 96(1), 1211–1218 (1977)
- Sellschopp, F.S., Arjona, M.A.: DC decay test for estimating d-axis synchronous machine parameters: A two-transfer-function approach. *IEE Proc. Electr Power Appl.* 153(1), 123–128 (2006)
- Yao, L., Sethares, W.A.: Nonlinear parameter estimation via the genetic algorithm. *IEEE Trans. on Signal Proc.* 42(1), 927–935 (1994)
- Liu, Z. H., et al.: Coevolutionary particle swarm optimization using AIS and its application in multi parameter estimation of PMSM. *IEEE Trans. Cybern.* 43(6), 1921–1935 (2013)
- Rezaie, J., Mehdi, G., Reza, F., et al.: Interior permanent magnet synchronous motor (IPMSM) adaptive genetic parameter estimation. *Proc. WCECS 2007*, 1–6 (2007)
- Song, Z., Jiang, G., Mei, X., et al.: A novel inertia identification method for servo system using genetic algorithm. *Int. Conf. Smart Grid and Electrical Automation (ICSGEA)*, pp. 22–25 (2016)
- Liu, K., et al.: Identification of flux linkage map of permanent magnet synchronous machines under uncertain circuit resistance and inverter nonlinearity. *IEEE Tran. Ind. Informat.* 14(2), 556–568 (2018)
- Pillay, P., Nolan, R., Haque, T.: Application of genetic algorithms to motor parameter determination for transient torque calculations. *IEEE Tran. Ind. Appl.* 33(5), 1273–1282 (1997)
- Price, K., Storn, R., Lampinen, J.: *Differential Evolution: A Practical Approach to Global Optimization*. Springer, Berlin (2005)
- Storn, R., Price, K.: Differential evolution - a fast and efficient heuristic for global optimization over continuous spaces. *J. of Global Optimization.* 11(4), 341–359 (1997)
- Tušar, T., Filipič, B.: Differential evolution versus genetic algorithm in multi-objective optimization. *Int. Conf. Evolutionary Multi-Criterion Optimization*, pp. 257–271 (2007)
- Das, S., Suganthan, P.N.: Differential evolution: A survey of the state-of-art. *IEEE Tran. Evol. Comput.* 15(1), 4–31 (2011)
- Mao, Y., Niu, S., Yang, Y.: Differential evolution-based multiobjective optimization of the electrical continuously variable transmission system. *IEEE Tran. Ind. Electron.* 65(3), 2080–2089 (2017)
- Deng, J., Mao, Y., Yang, Y.: Distribution power loss reduction of standalone DC microgrids using adaptive differential evolution-based control for distributed battery systems. *Energies* 13(9), 2129 (2020)
- Bhattacharya, A., Chattopadhyay, P.K.: Hybrid differential evolution with biogeography-based optimization for solution of economic load dispatch. *IEEE Tran. Power Syst.* 25(4), 1955–1964 (2010)
- Yang Y., Tan, S.C., Hui, S.Y.R.: Front-end parameter monitoring method based on two-layer adaptive differential evolution for SS-compensated wireless power transfer systems. *IEEE Tran. Ind. Informat.* 15(11), 6101–6113 (2019)
- Brest, J., et al.: Self-adapting control parameters in differential evolution: a comparative study on numerical benchmark problems. *IEEE Tran. Evol. Comput.* 6(10), 646–657 (2006)
- Rahman, K.M., Hiti, S.: Identification of machine parameters of a synchronous motor. *IEEE Tran. Ind. Appl.* 41(2), 557–565 (2005)

How to cite this article: Mao, Y., Niu, S., Yang, Y.: A new parameter identification method of a dual-rotor flux-modulation machine based on an adaptive differential evolution algorithm. *IET Renew. Power Gener.* 15, 1888–1897 (2021).

<https://doi.org/10.1049/rpg2.12112>